Controlled Surface Decoration with Functional Supramolecular Nanofibers by Physical Vapor Deposition

Dennis Schröder, Klaus Kreger, Ulrich Mansfeld, and Hans-Werner Schmidt*

Surface decoration of support structures by physical vapor deposition (PVD) of small molecular building blocks offers a versatile platform to realize functional supramolecular nanofibers in a controlled manner and with tailored properties. Here, details on the preparation of surface-decorated polyamide fabrics by PVD using N^1,N^3,N^5-tris[2-(diisopropylamino)-ethyl]-1,3,5-benzenetricarboxamide (1) as a molecular building block are reported. It is shown that a defined morphology with uniform nanofiber length can be achieved, which is controlled by the PVD conditions. The functional periphery of supramolecular nanofibers of 1 allows the immobilization of gold nanoparticles (AuNPs). This results in AuNP-loaded nanostructures with a high surface area, which can be used as a heterogenous catalyst for the reduction of 4-nitrophenol in aqueous media. The surface-decorated support structures with firmly deposited AuNPs also provide the opportunity to conveniently reuse these structures without compromising the catalytic performance. This approach provides fabrication strategies for the controlled surface decoration of macroscopic support structures with small molecular building blocks by PVD with the potential to realize functional robust supramolecular nanofibers for various catalytic or filtration applications.

1. Introduction

Fibrous materials with increased complexity gain growing interest due to their expanded property profile including flexibility and stiffness, controlled porosity, and high surface-to-volume ratio. Introducing different functionalities broadens the field of application including for example filter media with improved moisture permeability, and antiviral and antibacterial properties or

paves the way to novel applications including fibrous membranes for wearable electronics, energy generation, and energy storage as well as heterogeneous catalysis.[1–4]

The production of conventional and functional fibers based on polymer materials are performed by established top-down techniques from solution or melt.[5–7] In this context, electrospinning is one of the most extensively used techniques.[8–10] A way to improve or widen the characteristics toward multi-structured fibrous media is to combine different fiber types often based on different materials.[11] This includes for example the simultaneous electrospinning of two different polymer types resulting in a hierarchically structured fiber morphology.[12] Another example is based on one or two different polymers, consisting of an electrospun polymer fiber scaffold in which finely structured 2D nanofiber networks are embedded.[13–15]

Another approach is based on the combination of polymer fibers and supramolecular fibers. In contrast to top-down approaches, supramolecular fiber formation is based on a bottom-up strategy, namely the spontaneous self-assembly of dissolved small molecular building blocks from solution into fibrillar objects via secondary interactions. As a result, supramolecular fibers form in situ between an existing polymer fiber support. For example, we demonstrated the preparation of polymer/supramolecular fiber composites by immersing a polymer nonwoven in a solution of a 1,3,5-benzenetricarboxamide derivative (BTA) as a molecular building block and subsequent drying of the nonwoven.[16,17] These composites feature a significantly improved performance for the filtration of particulate matter. Hu et al. demonstrated the formation of a dual-nanonet of polymer nanofibers and supramolecular nanofibrils based on 1,3:2,4-di(3,4-dimethylbenzylidene) sorbitol.[18] These dual-nanonet filter media feature, besides a high moisture permeability, remarkable filtration efficiencies at low-pressure drops. In another approach, we prepared compact and shape-persistent sheets based on a network of functional supramolecular BTA nanofibers and polyacrylonitrile short fibers by a wet-laid technique.[19] The functional supramolecular nanofibers within the polymer fibers allow efficient immobilization of gold nanoparticles (AuNPs), which enables the use of the sheet as a reusable heterogeneous catalyst.

D. Schröder, K. Kreger, H.-W. Schmidt
Macromolecular Chemistry I and Bavarian Polymer Institute
University of Bayreuth
95440 Bayreuth, Germany
E-mail: hans-werner.schmidt@uni-bayreuth.de
U. Mansfeld
Bavarian Polymer Institute
University of Bayreuth
95440 Bayreuth, Germany

Apart from the combination of different fiber types, recent approaches make use of fibers with complex morphologies. For example, complex fiber morphologies based on central para-aramid fibers with off-standing nanofiber branches were demonstrated by Xu et al. They used chemical hydrolysis and physical shearing, which resulted in surface fibrillation of the central para-aramid fibers. These multiscale fiber morphologies feature outstanding filtration performance as well as good thermal insulation characteristics.[20,21] We demonstrated another approach to complex fiber morphologies based on a central polymer fiber with off-standing branches of supramolecular fibers. This morphology was realized by decorating the electrospun polymer fibers with seeds capable of initiating supramolecular fiber growth.[22] Similar polymer fiber/supramolecular branch – morphologies were realized by depositing suitable patches on the polymer fiber surface.[23,24] In particular for hierarchical structures based on such supramolecular and polymer fiber types, a distinct two-step procedure is required. In the first step, the seeds or patches were deposited on supporting polymer fibers. Subsequently, supramolecular fibers were grown from these seeds and patches, which acted as nucleation sites in a guided solution-based self-assembly process. Furthermore, in seed-initiated solution-based processes, it is challenging to achieve precise control over the supramolecular fiber length.

However, a fundamental aspect is how to precisely control the formation and morphology of polymer or supramolecular nanofibers at the interface on substrates. A promising approach that allows the defined surface decoration with tailored short fibers on substrates is based on chemical or physical vapor deposition (PVD), which has recently been demonstrated for various polymer and supramolecular materials.[25–29] In contrast to solution-based self-assembly processes, the use of additional tailored seeds is not required. In addition, the fiber length can be precisely controlled by the evaporation time.[29]

Another appealing aspect in this context is the introduction of functionality into the periphery of such fibers, which can ultimately be used for metal particle immobilization by attractive secondary interactions.

Here, we demonstrate the controlled surface decoration of a woven fabric with short and uniform functional supramolecular fibers by PVD (**Figure 1**). A polyamide fabric with defined fiber diameter and porosity was selected as model support. N^1,N^3,N^5-tris[2-(diisopropylamino)-ethyl]$-1,3,5$-benzenetricarboxamide (**1**) was selected as molecular building block, which is capable of forming supramolecular columns via three strands of hydrogen bonds. The supramolecular fibers feature an amino-functionalized surface suitable to efficiently immobilize gold nanoparticles (AuNPs) from the solution. We demonstrate that the AuNP-loaded mesostructured fabric can be beneficially used and reused as a heterogeneous catalyst in the model reaction, i.e., the reduction of 4-nitrophenol to 4-aminophenol.

2. Results and Discussion

2.1. Preparation of Supramolecular Nanofibers by PVD

1,3,5-Benzenetrisamides are a well-investigated class of supramolecular materials, which is characterized by the formation of three helical hydrogen bonds resulting in fiber-like
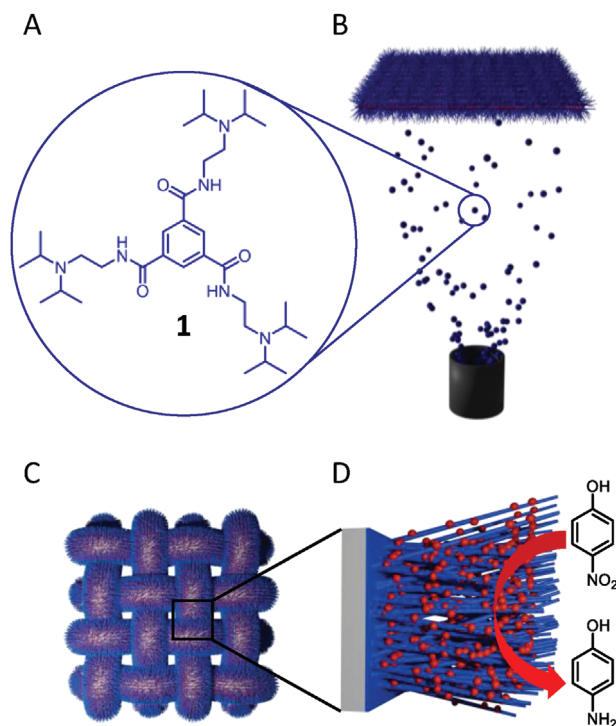

Figure 1. A) Chemical structure of the molecular building block, N^1,N^3,N^5-tris[2-(diisopropylamino)-ethyl]$-1,3,5$-benzenetricarboxamide 1. B) Schematic illustration of the PVD process. C) Corresponding woven fabrics decorated with supramolecular nanofibers of 1 prepared using PVD. D) The functional surface of the supramolecular nanofibers (in blue) on the woven fabric (in grey) allows the immobilization of AuNPs (in red) which can be used as heterogeneous catalysts for the reduction of 4-nitrophenol to 4-aminophenol in the presence of $NaBH_4$.

columnar assemblies.[30,31] Attaching short or bulky side aliphatic or aromatic groups to the amide groups typically leads to materials with high melting points and also high decomposition temperatures.[32] In particular, the latter is a prerequisite to be used in PVD processes. Recently, we have studied a 1,3,5-benzenetricarboxamide with peripheral functional side groups, i.e., N,N-diisopropylaminoethyl substituents (**1**, for details, see, Section S1, Supporting Information), those supramolecular fibers were capable of immobilizing metal nanoparticles.[24] The thermal properties, of this BTA derivative were determined by thermogravimetric analysis (TGA) and differential scanning calorimetry (DSC, see, Section S2, Supporting Information). TGA reveals no weight loss up to a temperature of ≈300 °C indicating a high thermal stability without decomposition into fragments. The DSC experiments yield a melting point of 275 °C and an isotropization temperature of 298 °C indicating the usability of **1** at evaporation temperatures below 300 °C. In the first set of PVD experiments, we found that **1** starts to evaporate at a temperature of 230 °C under a pressure of 10^{-6} mbar. Thus, the compound sublimes under these conditions. High performance liquid chromatography (HPLC) analysis of **1** after PVD compared to a sample before PVD shows only a single peak confirming that no decomposition takes place (see, Section S3, Supporting Information). In addition, we performed fourier transform infrared (FT-IR) spectroscopy before and after PVD (see, Section

S4, Supporting Information). The spectra are almost identical, which is in agreement with the findings of the HPLC analysis. Importantly, both FT-IR spectra feature amide A (N—H stretch vibration) at 3244 cm^{-1}, amide I (C=O stretch vibration) at 1638 cm^{-1}, and amide II (superposition of N—H bend and C—N stretch vibrations) at ≈1553 cm^{-1}. These vibrations indicate that hydrogen bonds are formed between the amide groups of BTA molecules ultimately resulting in a columnar arrangement of the BTAs.[33] Thus, vapor deposited **1** are present in an ordered fashion on the substrate. To investigate the morphology of the vapor-deposited BTAs, we performed a combinatorial PVD experiment on the same silicon substrate. For this, we applied the same conditions as used before; however, a shutter initially covering the substrate was moved by 1/5 at a given time resulting in a stepwise gradient. As a result, we received five individual sectors with a total vapor exposure time of 5, 10, 15, 30, and 45 min. For each sector, the morphology was analyzed using scanning electron microscopy (SEM) as depicted in **Figure** 2. During the first 5 min under these conditions, **1** appears to be deposited on the silicon substrate in a non-homogeneous droplet-like manner, which becomes a fully covered layer after 10 min. This initial formed layer, which is also referred to as a wetting layer, is often found as a deposit of small molecules prior to subsequent object formation. Consequently, this wetting layer acts as a nucleation sites for the supramolecular fiber growth. With increasing evaporation time, the supramolecular nanofiber growth proceeds largely perpendicular to the substrate in a roughly linear fashion resulting in a densely packed fiber mat. The fiber mat thickness ranges from ≈0.2 to 2.3 µm after evaporation time of 10 to 45 min. Both aspects, the initially formed layer of nucleation sites and the adjustable evaporation time at a constant building block feed allow precise control of the supramolecular fiber length, in contrast to solution-based self-assembly processes.

2.2. Surface Decoration of Woven Fabrics with Defined Supramolecular Nanofibers

Woven or nonwoven fabrics are mechanically stable fibrous porous structures. Thus, these fabrics can be regarded as macroscopic support materials with a high surface-to-volume ratio, which are readily accessible by liquid media. In contrast to nonwovens, woven fabrics are characterized by their defined geometry including the fiber diameter and the pore size and shape, which we use as a model support structure. Here, we have selected a mono-layered interwoven polyamide fabric with a fiber diameter of 35 µm and mesh width of 50 µm (see, Section S5, Supporting Information). To prepare a fully surface-decorated woven fabric with BTA nanofibers, square pieces of 7.6 cm × 7.6 cm were placed in the vapor deposition chamber. PVD was performed at a pressure of 10^{-6} mbar and a source temperature of 230 °C for 120 min. To ensure complete coverage of both sides of the fabric, the support was flipped by 180° and the PVD process was repeated. The morphology of the vapor-deposited supramolecular nanofiber on the woven fabric was investigated by scanning electron microscopy and is depicted in **Figure** 3. The overview image reveals that the entire polyamide fabric is densely and homogeneously covered with supramolecular BTA nanofibers
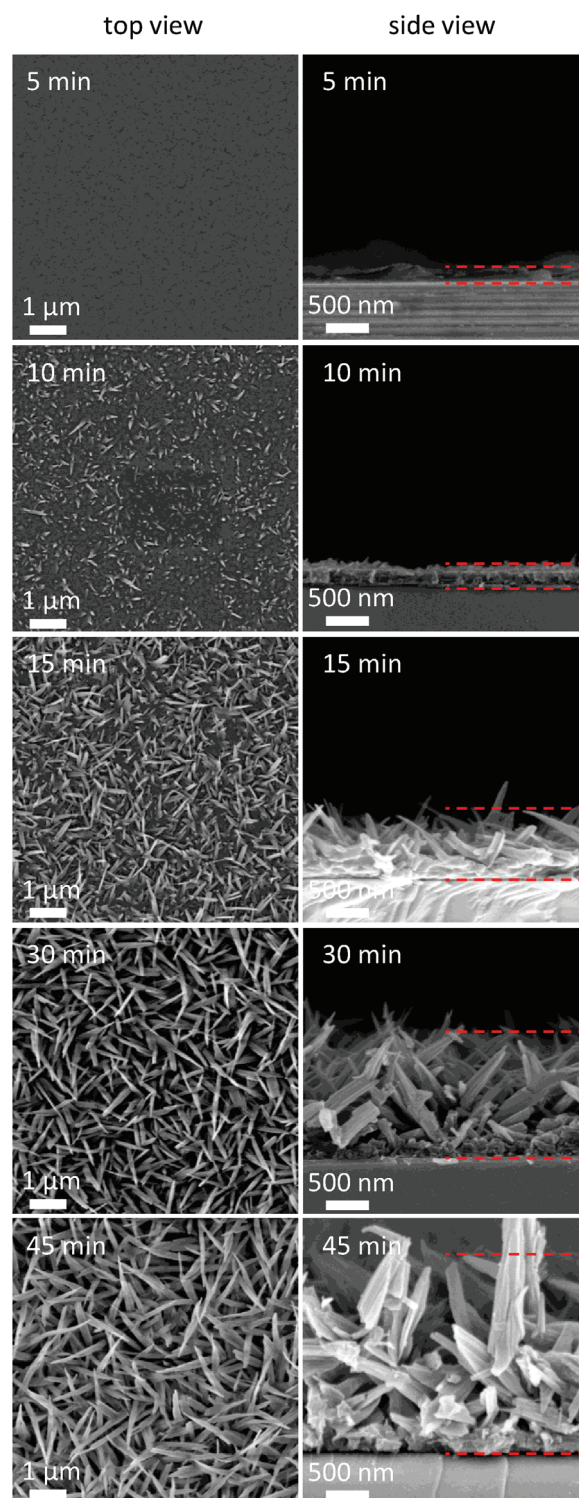

Figure 2. SEM images of vapor deposited **1** on the same silicon wafer at different evaporation times in a combinatorial approach of the PVD experiment comprising five different sectors (evaporation rate = 1.4 µg s^{-1}, T$_{source}$ = 230, T$_{substrate}$ = 25 °C). The five different vapor exposure times, i.e., 5, 10, 15, 30, and 45 min, were realized by successively covering the substrate with a shutter for the given time. The left column shows top view images and the right column side views images. Dashed red lines in the side view images are a guide to the eye indicating the height of deposited fiber mat of **1** ranging from 0.2 µm (for 5 min) to 2.3 µm (for 45 min).

**ADVANCED
SCIENCE NEWS**

www.advancedsciencenews.com

**ADVANCED
MATERIALS
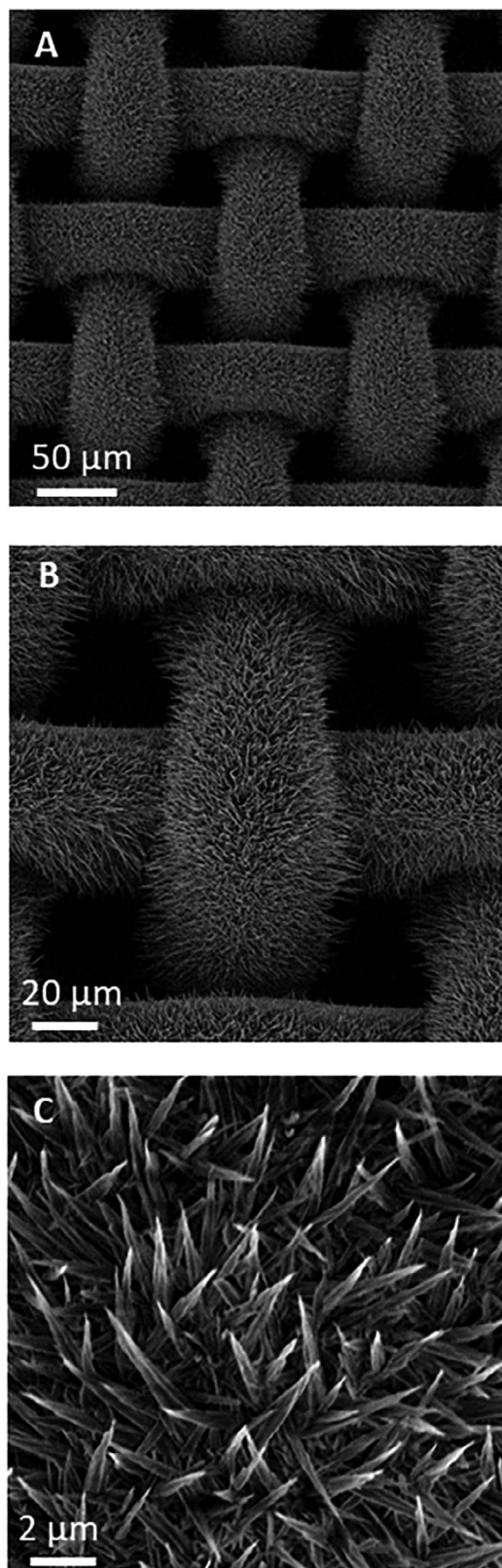INTERFACES**
Open Access

www.advmatinterfaces.de

Figure 3. SEM micrographs of surface-decorated woven fabrics with defined supramolecular nanofibers. A) Overview image and B, C) different magnifications of the polyamide woven fabric with fibers of 1. PVD conditions: $T_{source} = 230$, $T_{substrate} = 25$ °C. $p = 10^{-6}$ mbar, deposition time 120 min.

(Figure 3A). At larger magnifications it can be seen (Figure 3B,C), that the supramolecular nanofibers of the vapor-deposited building blocks were grown perpendicularly from the surface of the support structure, in a similar manner as observed before for the solid silicon substrate. Additionally, the nanofiber morphology of **1** was found to be almost identical when viewed from either the front or back side of the woven fabric (see, Section S6, Supporting Information). This indicates that the nanofiber formation via PVD is a robust and reproducible process. This was also demonstrated by several repetitions of the PVD experiment with other neat woven fabrics of the same kind. From these images, we were able to estimate a supramolecular fiber diameter of ≈350 nm. Yet, the nanofiber length after 120 min of evaporation cannot be clearly recognized. Owing to the defined structure of the woven fabric, we were able to superimpose a neat woven fabric with a surface-decorated fabric with a high degree of accuracy. This allows us to identify the starting point of the nanofiber growth as well as the ending of the supramolecular nanofibers. Applying these processing conditions, we determine a uniform length of the supramolecular BTA fibers to be 8 µm (see, Section S7, Supporting Information).

2.3. Immobilization of AuNPs on the Supramolecular Nanofibers

To demonstrate the use of the functional periphery of the supramolecular nanofibers decorated on the fabric, we investigate the immobilization of AuNPs. For this purpose, we synthesized AuNPs according to the well-established procedure of Gittins and Caruso.[34] This involves the reduction of tetrachloroauric(III) acid in toluene and subsequent stabilization and transfer to aqueous media using dimethylaminopyridine (DMAP) as a non-acidic ligand. UV/vis spectroscopy of the dark red solution in water shows an absorption maximum at 520 nm attributed to plasmon resonance of the AuNPs (see, Section S8, Supporting Information). Using dynamic light scattering (DLS) we found a uniform particle size distribution and no indication for agglomerates. The average diameter of the AuNPs was found to be ≈10 nm. We used this aqueous solution to immobilize the DMAP-stabilized AuNPs on the functional surface of the short supramolecular nanofibers on the woven fabric by dipping the mesostructured fabric into the AuNPs dispersion. To remove non-immobilized AuNPs, the fabric was washed with water and then dried. SEM investigations of the AuNP-loaded surface-decorated woven fabrics reveal that the overall morphology of mesostructured woven fabric remains largely unchanged (**Figure 4A,B**). The first evidence for successful deposition of the AuNPs on the supramolecular nanofibers was obtained by using a back-scatter detector during SEM. This results in bright features on top of the supramolecular nanofibers in the micrographs, which is indicative of the presence of metal particles. Since the mesostructured woven is very densely packed with supramolecular nanofibers, no statement can be made on the AuNPs immobilization capability of the polyamide woven support (Figure 4C,D). Thus, we used a neat polyamide woven fabric as a reference and immersed it in the AuNPs dispersion followed by a washing step; however, no AuNPs were found on the fabric demonstrating the importance of the functional periphery of the supramolecular nanofibers for the AuNPs
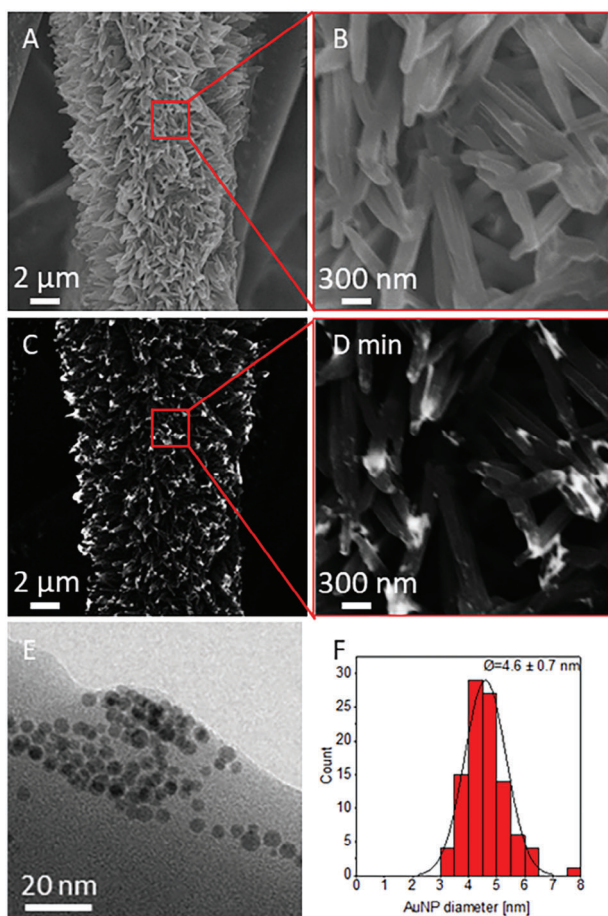
**ADVANCED
SCIENCE NEWS**

www.advancedsciencenews.com

**ADVANCED
MATERIALS
INTERFACES**
Open Access

www.advmatinterfaces.de

Figure 4. A,B) SEM images at different magnifications of AuNP decorated mesostructured woven using an Inlens detector. C,D) SEM images at different magnifications using the same woven and a backscatter electron detector reveal bright areas on top of the supramolecular fibers indicating the presence of gold particles. E) Distinct individual AuNPs on mechanically detached supramolecular nanofibers as revealed by TEM featuring a uniform particle size distribution. F) Corresponding histogram of the diameter of the immobilized AuNPs determined by evaluating 100 particles showing an average particle diameter of 4.6 ± 0.7 nm.

immobilization. After detaching and transferring small fragments of supramolecular nanofibers with immobilized AuNPs onto substrates, we investigated several nanofibers by transmission electron microscopy (TEM, Section S9, Supporting Information). TEM micrographs of different fibers reveal that distinct AuNPs on the supramolecular fibers are present, which appear to be arranged in a thread-like manner. At higher magnifications, small non-agglomerated AuNPs with uniform particle size distribution were identified (Figure 4E; Section S9, Supporting Information). The average diameter of the immobilized AuNPs was determined to be 4.7 nm (Figure 4F). Compared to the diameter of the as-prepared AuNPs determined by DLS, this value is smaller by a factor of about two, which is attributed to an overestimation of DLS values.[35] To determine the amount of AuNPs that is loaded onto the surface-decorated woven fabric, we performed inductively coupled plasma-optical emission spectrometry (ICP-OES). Three individual samples each for the

mesostructured woven were analyzed yielding a gold content of 21 µg.

2.4. Immobilized AuNPs on Mesostructured Woven Support for Heterogeneous Catalysis

Ultimately, we investigated the surface-decorated woven fabrics loaded with AuNPs as heterogeneous catalysts for the reduction of 4-nitrophenol to 4-aminophenol in the presence of $NaBH_4$. The AuNP-catalyzed reduction of 4-nitrophenol is a frequently studied model reaction in which the degree of conversion can be readily investigated by UV–vis spectroscopy. In this case, the reaction kinetics are monitored by following the progression of the absorption at 400 nm. This absorption is attributed to the sodium 4-nitrophenolate, which is immediately formed by the addition of a large excess of $NaBH_4$. In the presence of the AuNP catalyst, the absorption of 4-nitrophenolate is steadily decreasing and simultaneously a new absorption at ≈300 nm is increasingly established due to the formation of 4-aminophenolate (**Figure 5A**). The decrease in the reactant, i.e., sodium 4-nitrophenolate, (c_t/c_0) over time with and without the immobilized AuNP catalyst is plotted in Figure 5B. As anticipated, the absence of AuNPs precludes any discernible conversion. In contrast, the immobilized AuNP catalyst on the woven support facilitates a rapid reaction, resulting in a conversion of up to 95% within 4 min. The progression of the conversion, as illustrated in Figure 5B, also indicates that the reaction rate of the 4-nitrophenol reduction to 4-aminophenol follows pseudo-first-order kinetics, which is related to the substantial excess of $NaBH_4$. Consequently, plotting $-\ln(c_t/c_0)$ over time revealed a linear relationship (Figure 5C). The apparent kinetic reaction rate constants (k_{app}) were derived from the slope of the linear regression and found to be $k_{app} = 1.16$ min^{-1}. Compared to previously reported k_{app} values on reusable fiber-based systems in literature,[36–40] and in particular to our recent findings,[19] this k_{app} seems to be relatively high. With respect to the latter AuNP-loaded supramolecular/polymer fiber composite, this finding may be attributed to easier accessibility to reactive catalytic sites.

An important feature of deposited AuNPs on macroscopic supports is the potential to remove and reuse the heterogeneous catalysts while the catalytic activity is maintained. To verify the reusability, we performed three consecutive cycles of the catalysis experiments. For each cycle, the same round-shaped AuNP-loaded mesostructured woven fabric was immersed in a freshly prepared reaction mixture containing 4-nitrophenol and removed after completion of the reduction to 4-aminophenol as confirmed by absorption measurements. Figure 5D depicts the progress of the reaction by absorption measurements over time for three consecutive runs. In all three cycles, the time to complete the reaction as well as the k_{app} remains the same. Consequently, a reduction in the catalytic activity of the supramolecular nanofiber carrying the AuNPs cannot be observed. This indicates that the morphology of the supramolecular nanofiber remains intact. This also indicates that the AuNPs on the supramolecular nanofiber maintain their reactivity and do not leach to the solution.

To verify these findings, we conducted SEM, TEM, and ICP-OES measurements on dried samples (see, Section S10,
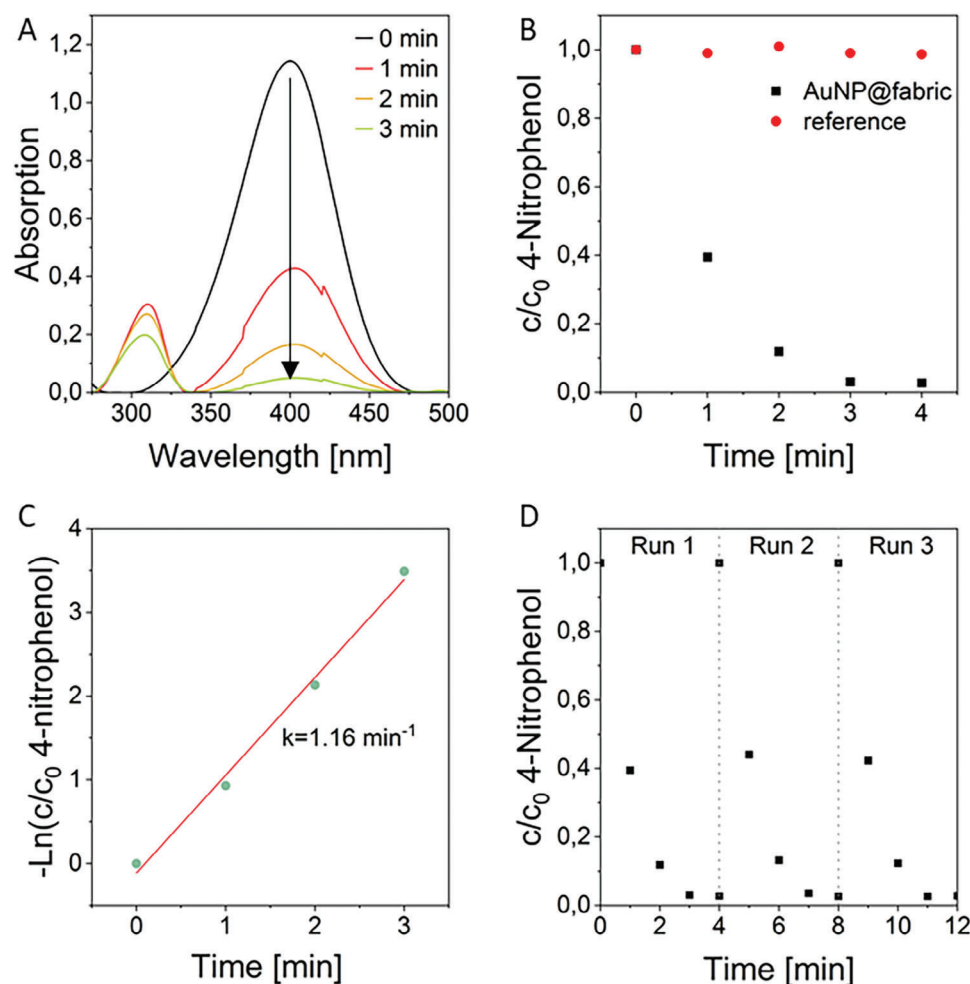
ADVANCED
SCIENCE NEWS

www.advancedsciencenews.com

ADVANCED
MATERIALS
INTERFACES
Open Access

www.advmatinterfaces.de

Figure 5. A) Temporal evolution of UV/vis spectra recorded from 250 to 500 nm during the reduction of 4-nitrophenolate to 4-aminopenolate using $NaBH_4$ and AuNP decorated mesostructured woven as heterogenous catalyst. B) Decrease of the 4-nitrophenolate concentration (c_t/c_0) over time with and without AuNP-deposited catalyst on mesostructured woven fabric. C) Determination of k_{app} from the slope of the linear regression. D) Reusability experiments of the AuNP decorated mesostructured woven in three consecutive catalytic cycles. Reaction conditions for (A–D): 1.5 mL of 0.1 mM aqueous 4-nitrophenol solution, 1.5 mL of 100 mM aqueous $NaBH_4$, and 21 µg of immobilized AuNPs on mesostructured woven fabrics. The reaction is performed at 25 °C with stirring at 600 rpm.

Supporting Information). The SEM micrographs demonstrate that the surface-decorated morphology remains intact, with no significant change observable. This indicates a strong adhesion of supramolecular nanofibers to the woven fabric. Similarly, TEM of fragments of supramolecular nanofibers revealed a similar picture of deposited AuNPs with an average size of 4.7 nm, indicating that the AuNPs are firmly immobilized. This finding is consistent with ICP-OES analysis of the reaction solution after catalysis, which showed no gold within the detection limit of the method.

3. Conclusion

Here, we presented a feasible approach to realize tailored surface-decorated support structures by PVD comprising uniform supramolecular nanofibers based on N^1,N^3,N^5-tris[2-(diisopropylamino)-ethyl]−1,3,5-benzenetricarboxamide (**1**) and a polyamide woven fabric. Unlike solution-based self-assembly processes, the PVD process enables precise control of the supramolecular fiber length on different substrates without the use of pre-deposited seeds. The functional periphery of supramolecular nanofibers of **1** facilitates a robust immobilization of AuNPs, which can be used as a heterogeneous catalyst for the reduction of 4-nitrophenol. The catalytic reaction proceeds with an k_{app} of 1.16 min^{-1}, which we attribute to ready accessibility to the reactive catalytic sites on the surface-decorated support. Beneficially, such surface-decorated fabrics with immobilized AuNPs, be easily removed and reused without compromising the catalytic performance due to the robust mechanical stability of and between the integral components. We anticipate that the tailored preparation of surface-decorated support structures by PVD can be conveniently transferred to other functional uniform supramolecular BTA nanofibers. The rational design of the functional BTA could pave the way to the development of mesostructured surfaces for various applications in (photo)catalysis, filtration, or antibacterial coatings.

**ADVANCED
SCIENCE NEWS**

www.advancedsciencenews.com

**ADVANCED
MATERIALS
INTERFACES**
Open Access

www.advmatinterfaces.de

4. Experimental Section

Preparation of Supramolecular Nanofibers of 1 on Substrates by PVD:
For PVD of **1**, a modified vapor deposition chamber PLS 500 from Balzers was used. Quartz crystal sensors were mounted near the substrate holder and used to monitor the evaporation rate. About 500 mg of **1** was weighed into a quartz crucible, which was placed into an effusion cell used as a heating source. As substrate a silicon wafer was used. At 230 °C temperature of the effusion cell and 10^{-6} mbar, a constant apparent evaporation rate was monitored by the quartz crystal sensors and found to be 1.4 µg s^{-1}. For the preparation of step thickness gradients, a combinatorial set-up was used to obtain five different sectors by moving a shutter at a distinct distance in a similar manner as described previously.[29] At the end of each experiment, the vacuum chamber was ventilated with air.

Surface Decoration of Woven Fabrics with Defined Supramolecular Nanofibers of 1: For the preparation of a fully surface-decorated woven fabric with BTA nanofibers, the same PVD setup as outlined above was used. As support material, a polyamide woven fabric with a uniform fiber diameter of 35 µm and a mesh width of 50 µm was used and cut into a square piece of 7.6 cm × 7.6 cm having a mass of ≈200 mg. The cut piece of the fabric was clamped into a custom-made 3D-printed holder and fixated in a substrate holder, which was located ≈35 cm above the effusion cells in the vapor deposition chamber. A closed shutter covers the substrate holder prior to the evaporation process. PVD was initiated at a pressure of 10^{-6} mbar and a source temperature of 230 °C of the effusion cell. A constant evaporation rate was monitored by quartz crystal sensors and determined to be 1.4 µg s^{-1}. The shutter was fully opened and after an evaporation time of 240 min, the chamber was ventilated with air, opened and the custom-made holder was flipped by 180°. Subsequently, the process was repeated to ensure complete coverage of both sides of the mono-layered woven fabric with supramolecular nanofibers.

Gold Nanoparticle Loading: AuNP immobilization on the supramolecular nanofibers was done by dipping a round-shaped piece of mesostructured woven with a diameter of 12 mm (m = 720 µg) into an aqueous dispersion of the freshly prepared DMAP-stabilized AuNPs for 1 h. After deposition of the AuNPs, the woven fabric was removed from the immersion solution and washed with ultrapure water until an excess of non-immobilized AuNPs was removed. The AuNP-loaded woven fabric was subsequently dried in a vacuum (<5 mbar) at 40 °C for 15 h.

UV/vis Spectroscopy: Absorption measurements were performed on a Jasco Spectrometer V-670 with a scan speed of 400 nm min^{-1} at 25 °C using a quartz glass cuvette (D = 10 mm). Baseline correction was carried out by measuring a blank sample with Milli-Q water before measurements.

SEM: Scanning electron microscopy was performed with a Zeiss 1530 FESEM at 3 kV using an Inlens detector. Samples were fixed via a double-sided adhesive conductive carbon tape on an SEM sample holder and subsequently sputtered with platinum (2 nm) prior to SEM investigation. For visualization of AuNP a back-scatter detector was used at 10 kV.

TEM: Transmission electron microscopy was performed on a JEOL JEM-2200FS. For the investigation of the AuNPs distribution on the supramolecular fibers, a lacey carbon-coated copper grid (LC400, EMS, USA) was wiped over the surface of the mesostructured woven to transfer supramolecular fiber fragments on the TEM grid. The same procedure was applied for the analysis of the AuNP size distribution on a mesostructured woven after that was used three times in the catalytic reduction of 4-nitrophenol. All samples were investigated at room temperature using the bright-field mode with energy filtering at an acceleration voltage of 200 kV.

ICP-OES: Inductively coupled plasma-optical emission spectrometry measurements were carried out using a PerkinElmer Avio 200 equipped with an S10 autosampler, Echelle polychromator, Argon humidifier, and a DBI-CCD detector. The samples were calibrated against a single gold standard (PerkinElmer Pure, Gold 1000 mg L^{-1} in 10% HCl) with concentrations of 0.05, 0.1, 0.5, 1, and 10 mg L^{-1}, respectively. For sample preparation, the AuNP solution before and after immersion of the mesostructured woven fabrics as well as the reaction solutions after catalysis was evaporated completely at 70 °C, dissolved in 0.5 mL of aqua regia, and diluted with 9.5 mL of deionized water (18.2 MΩ cm).

Reduction of 4-Nitrophenol by AuNP-Loaded Mesostructured Woven Fabrics as Heterogeneous Catalyst: The catalytic activity of the AuNP-loaded mesostructured woven fabrics was examined by the reduction of 4-nitrophenol to 4 aminophenol. For this, 1.5 mL of a 0.1 mm 4-nitrophenol solution and 1.5 mL of a 100 mm NaBH$_4$ solution were put in a quartz cuvette. Subsequently, a round-shaped Au-loaded woven fabric with a diameter of 13 mm was completely immersed in the reaction solution using a tweezer. Then the reaction was stirred at 25 °C and 600 rpm for 15 min. The progress of the reaction was monitored by absorption measurements taken every minute in the range of 250–500 nm with a scan speed of 400 nm min^{-1}.

Supporting Information

Supporting Information is available from the Wiley Online Library or from the author.

Acknowledgements

Conflict of Interest

The authors declare no conflict of interest.

Data Availability Statement

The data that support the findings of this study are available from the corresponding author upon reasonable request.

Keywords

[1] E. Loccufier, D. P. Debecker, D. R. D'hooge, K. de Buysser, K. de Clerck, *ChemCatChem* **2024**, 202301563, https://doi.org/10.1002/cctc.202301563.

[2] C. Chen, J. Feng, J. Li, Y. Guo, X. Shi, H. Peng, *Chem. Rev.* **2023**, *123*, 613.

[3] J.-W. Jung, C.-L. Lee, S. Yu, I.-D. Kim, *J. Mater. Chem. A* **2016**, *4*, 703.

[4] X. Li, Z.-H. Lin, G. Cheng, X. Wen, Y. Liu, S. Niu, Z. L. Wang, *ACS Nano* **2014**, *8*, 10674.

**ADVANCED
SCIENCE NEWS**

www.advancedsciencenews.com

**ADVANCED
MATERIALS
INTERFACES**
Open Access

www.advmatinterfaces.de

[5] C. J. Ellison, A. Phatak, D. W. Giles, C. W. Macosko, F. S. Bates, *Polymer* **2007**, *48*, 3306.

[6] E. S. Medeiros, G. M. Glenn, A. P. Klamczynski, W. J. Orts, L. H. C. Mattoso, *J. Appl. Polym. Sci.* **2009**, *113*, 2322.

[7] J. G. McCulloch, *Int. Nonwovens J.* **1999**, *os-8*, 139.

[8] A. Greiner, J. H. Wendorff, *Angew. Chem., Int. Ed.* **2007**, *46*, 5670.

[9] M. Bognitzki, W. Czado, T. Frese, A. Schaper, M. Hellwig, M. Steinhart, A. Greiner, J. H. Wendorff, *Adv. Mater.* **2001**, *13*, 70.

[10] J. Xue, T. Wu, Y. Dai, Y. Xia, *Chem. Rev.* **2019**, *119*, 5298.

[11] T. Lu, J. Cui, Q. Qu, Y. Wang, J. Zhang, R. Xiong, W. Ma, C. Huang, *ACS Appl. Mater. Interfaces* **2021**, *13*, 23293.

[12] S. Zhang, H. Liu, X. Yin, J. Yu, B. Ding, *ACS Appl. Mater. Interfaces* **2016**, *8*, 8086.

[13] H. Liu, S. Zhang, L. Liu, J. Yu, B. Ding, *Adv. Funct. Mater.* **2019**, *29*, 1904108.

[14] S. Zhang, H. Liu, N. Tang, S. Zhou, J. Yu, B. Ding, *Adv. Mater.* **2020**, *32*, 2002361.

[15] X. Xu, S. Liu, X. Liu, J. Yu, B. Ding, *J. Colloid Interface Sci.* **2024**, *657*, 463.

[16] H. Misslitz, K. Kreger, H.-W. Schmidt, *Small* **2013**, *9*, 2053.

[17] D. Weiss, D. Skrybeck, H. Misslitz, D. Nardini, A. Kern, K. Kreger, H.-W. Schmidt, *ACS Appl. Mater. Interfaces* **2016**, *8*, 14885.

[18] M. Hu, Y. Wang, Z. Yan, G. Zhao, Y. Zhao, L. Xia, B. Cheng, Y. Di, X. Zhuang, *J. Mater. Chem. A* **2021**, *9*, 14093.

[19] M. Drummer, C. Liang, K. Kreger, S. Rosenfeldt, A. Greiner, H.-W. Schmidt, *ACS Appl. Mater. Interfaces* **2021**, *13*, 34818.

[20] K. Xu, J. Deng, R. Lin, H. Zhang, Q. Ke, C. Huang, *J. Mater. Chem. A* **2020**, *8*, 22269.

[21] K. Xu, J. Deng, G. Tian, L. Zhan, J. Ma, L. Wang, Q. Ke, C. Huang, *Nano Res.* **2022**, *15*, 5695.

[22] M. Burgard, D. Weiss, K. Kreger, H. Schmalz, S. Agarwal, H.-W. Schmidt, A. Greiner, *Adv. Funct. Mater.* **2019**, *29*, 1903166.

[23] A. Frank, C. Hils, M. Weber, K. Kreger, H. Schmalz, H.-W. Schmidt, *Angew. Chem., Int. Ed.* **2021**, *60*, 21767.

[24] A. Frank, M. Weber, C. Hils, U. Mansfeld, K. Kreger, H. Schmalz, H.-W. Schmidt, *Macromol. Rapid Commun.* **2022**, *43*, 2200052.

[25] D. Varadharajan, K. Nayani, C. Zippel, E. Spuling, K. C. Cheng, S. Sarangarajan, S. Roh, J. Kim, V. Trouillet, S. Bräse, N. L. Abbott, J. Lahann, *Adv. Mater.* **2022**, *34*, 2108386.

[26] K. C. K. Cheng, M. A. Bedolla-Pantoja, Y.-K. Kim, J. V. Gregory, F. Xie, A. de France, C. Hussal, K. Sun, N. L. Abbott, J. Lahann, *Science.* **2018**, *362*, 804.

[27] L. Adler-Abramovich, D. Aronov, P. Beker, M. Yevnin, S. Stempler, L. Buzhansky, G. Rosenman, E. Gazit, *Nat. Nanotechnol.* **2009**, *4*, 849.

[28] N. Amdursky, M. Molotskii, D. Aronov, L. Adler-Abramovich, E. Gazit, G. Rosenman, *Nano Lett.* **2009**, *9*, 3111.

[29] D. Schröder, C. Neuber, U. Mansfeld, K. Kreger, H.-W. Schmidt, *Small Sci* **2023**, *4*, 2300160.

[30] M. P. Lightfoot, F. S. Mair, R. G. Pritchard, J. E. Warren, *Chem. Commun.* **1999**, *19*, 1945.

[31] S. Cantekin, T. F. A. de Greef, A. R. A. Palmans, *Chem. Soc. Rev.* **2012**, *41*, 6125.

[32] M. Blomenhofer, S. Ganzleben, D. Hanft, H.-W. Schmidt, M. Kristiansen, P. Smith, K. Stoll, D. Mäder, K. Hoffmann, *Macromolecules* **2005**, *38*, 3688.

[33] P. J. M. Stals, M. M. J. Smulders, R. Martín-Rapún, A. R. A. Palmans, E. W. Meijer, *Chem. – A Eur. J.* **2009**, *15*, 2071.

[34] D. I. Gittins, F. Caruso, *Angew. Chem., Int. Ed.* **2001**, *40*, 3001.

[35] H. Hinterwirth, S. K. Wiedmer, M. Moilanen, A. Lehner, G. Allmaier, T. Waitz, W. Lindner, M. Lämmerhofer, *J. Sep. Science* **2013**, *36*, 2952.

[36] M. Abbas, H. H. Susapto, C. A. E. Hauser, *ACS Omega* **2022**, *7*, 2082.

[37] X. Cao, S. Yan, F. Hu, J. Wang, B. Sun, Z. Xiao, *RSC Adv.* **2016**, *6*, 64028.

[38] N. Guarrotxena, L. Garrido, I. Quijada-Garrido, *Adv. Mater. Interfaces* **2018**, *5*, 1801374.

[39] J. Li, C. Liu, Y. Liu, *J. Mater. Chem.* **2012**, *22*, 8426.

[40] K. Sawada, S. Sakai, M. Taya, *J. Mater. Sci.* **2014**, *49*, 4595.

2400259 (8 of 8)